PCCP

ROYAL SOCIETY OF CHEMISTRY

PAPER

View Article Online
View Journal



Cite this: DOI: 10.1039/d5cp02933c

# Zinc-mediated multimerization of the N-terminal CCHC zinc finger domain of BCL11B: a key to stability and a potential therapeutic target

Anne Susemihl,[ab] Felix Nagel,[a] Piotr Grabarczyk,[b] Christian Andreas Schmidt[b] and Mihaela Delcea *[a]

The transcription factor B cell lymphoma/leukemia 11B (BCL11B) homomultimerizes *via* its N-terminal CCHC-type zinc finger domain. Our previous findings revealed that BCL11B forms tetramers, rather than the initially predicted dimers. This requires a deeper understanding of the nature of these higher-order interactions. Here, we present a comprehensive biophysical characterization of the wild-type domain and selected mutants, with a focus on their dependency on $Zn^{2+}$ for structure, stability, and multimerization. The mutations were selected to probe the role of hydrophobic interactions (I70A), and to alter the zinc coordination sphere to CCCC (H76C), or the more common C2H2 motif (C81H). Size exclusion chromatography showed higher-order complexes with $Zn^{2+}$, and circular dichroism spectroscopy revealed a typical zinc finger fold. Both complex size and secondary structure were reversibly altered by $Zn^{2+}$ removal and re-addition. Melting temperature analysis showed that $Zn^{2+}$-bound species are more stable, with tetrameric complexes exhibiting higher thermal stability than dimers. Isothermal titration calorimetry indicated that tetrameric species have higher affinities to $Zn^{2+}$ than dimers. The I70A mutation, located outside the canonical zinc coordination sphere, affected zinc binding affinity and multimerization. Substitution with $Co^{2+}$, monitored by UV-vis spectroscopy, confirmed the tetrahedral coordination geometry and revealed differences in half-lives among the variants. These findings emphasize the central role of $Zn^{2+}$, suggesting a cooperative effect between hydrophobic interactions, multimerization, and zinc binding stability. The dynamic and reversible nature of $Zn^{2+}$-mediated folding and assembly highlights this domain as a potential therapeutic target. Our study provides a foundation for future strategies that aim to target the degradation of BCL11B.

Received 31st July 2025,
Accepted 14th November 2025

DOI: 10.1039/d5cp02933c

rsc.li/pccp



## Introduction

Zinc finger domains represent some of the most common DNA binding motifs in eukaryotic transcription factors, occupying a central role in gene regulation.[1–4] The first identified zinc finger was the transcription factor IIIa in *Xenopus laevis* in the late 1980s.[1] Since then, the number of identified zinc finger proteins has increased drastically, with an estimated 5% of genes being zinc finger proteins encoded in the human genome.[5,6] Structurally, zinc fingers are characterized by their central zinc ion ($Zn^{2+}$), which is classically coordinated by histidine and cysteine residues.[7–9] The zinc finger motif $C_2H_2$, coordinating the $Zn^{2+}$ with each two histidine and two cysteine residues, is the most frequently and best described zinc finger motif.[10] Another motif is the CCHC zinc finger, with three coordinating cysteine and one histidine residue. Both motifs are structurally very similar, but the latter is less frequently described and studied.[11,12]

Being relevant in gene regulation, a plethora of zinc finger proteins are linked to different diseases, especially involved in cancer onset and progression and all principal pathways of cancer progression, carcinogenesis to metastasis formation.[13–15] The structural and functional significance of zinc finger domains render them attractive targets in the development of new therapeutics, especially with metal-based compounds. Cobalt inhibitors, such as Co(III)–Schiff-base complexes ([Co(III)SB(Im)2]), have been developed, with an inhibiting effect on Krüppel-like transcription factors. They have been shown to have therapeutic potential in psoriasis, herpes, and sexually transmitted diseases.[16] Zinc finger proteins can act as tumor suppressors and/or oncogenes.[4,14,17–19]

A protein that functions as both an oncogene and a tumor suppressor is the Krüppel-like transcription factor B cell lymphoma/leukemia 11B (BCL11B).[20–22] BCL11B plays a role in the

[a] *Department of Biophysical Chemistry, Institute of Biochemistry, University of Greifswald, Greifswald, Germany. E-mail: delceam@uni-greifswald.de*
[b] *Internal Medicine C, University Medicine Greifswald, Greifswald, Germany*

differentiation of CD4+ CD8− T helper cells and CD4− CD8+ cytotoxic T cells; its involvement in NK cells has also been described.[23–26] Post-translational modifications play a decisive role in its function. While SUMOylation enables the recruitment of co-activator p300 and activated target genes such as Id2, phosphorylation impairs BCL11B's interaction with the NuRD complex, thereby facilitating p300 recruitment and converting BCL11B from a repressor to an activator. Additionally, SUMOylation can promote the degradation of BCL11B and therefore, decrease the expression of T cell associated genes.[27] Human genetic studies suggest the role of BCL11B as a tumor suppressor in T cells. Chromosomal rearrangements resulting in a loss of function, were identified in ∼10% of the studied T-ALL cases.[28] A role in skin cancer is also discussed[29] and overexpression of BCL11B was reported in all stages of mycosis fungoides (MF). Treatment with interferon was shown to reduce BCL11B expression and enhance cell death.[30]

The N-terminal zinc finger domain (ZF0) of BCL11B is involved in protein–protein interactions, and enables the self-association of proteins to homomultimers.[31] Crucially, our previous research[32] demonstrated that this atypical CCHC domain forms larger complexes than previously anticipated, specifically tetramers, instead of the commonly assumed dimers.[31] This observation was independently supported by another group, who reported tetramer formation for the highly homologous BCL11A.[33] Additionally, the ZF1 (residues 221–251) seems to promote dimerization.[34]

Given these unexpected higher-order assemblies, there was a clear need for further understanding of the nature of these protein–protein interactions. Especially in the context of T-ALL, a difficult-to-treat cancer type,[35] the zinc finger mediated multimerization might be of great importance. Targeted degradation of BCL11B could be a promising therapeutic strategy. Therefore, a deeper understanding of this small N-terminal zinc finger domain ($BCL11B_{42–94}$) is an important step towards developing new approaches for targeted degradation.

Here, we report a comprehensive study of the N-terminal BCL11B CCHC zinc finger domain regarding its zinc ion binding properties and the influence of $Zn^{2+}$ on the complex size, structure, and stability. Through a detailed investigation utilizing size exclusion chromatography, circular dichroism spectroscopy, isothermal titration calorimetry, and UV-vis measurements, we aim to lay the groundwork and deepen the understanding of the multimerization process and to potentially enable future drug targeting strategies.

## Materials and methods

Chemicals were purchased from Sigma-Aldrich (Taufkirchen, Germany), unless stated otherwise. Prior to use, all buffers were filtered through 0.22 μm nitrocellulose membranes (GVS, Sanford, USA) and degassed using an ultrasonic bath (Elmasonic S30H, Elma, Singen, Germany).

### Protein expression and purification

The small zinc finger domain $BCL11B_{42–94}$ was purified as previously described.[36] In brief, $BCL11B_{42–94}$ WT in a customized vector provided *via* VECTORBUILDER (Vectorbuilder Inc., Santa Clara, CA, USA) was equipped with a fluorescent CyPet-tag, a hexahistidine ($His_6$)-tag, a tobacco etch virus (TEV) cleaving site and an ampicillin (Amp) resistance. The integrated restriction enzyme sites KpnI and XhoI were used to prepare the mutants. Mutant DNA was ordered as gBlocks (Integrated DNA Technologies, Leuven, Belgium), and digested with the respective restriction enzymes. Following the manual's instructions for T4 ligase (Carl Roth, Karlsruhe, Germany), the prepared mutant DNA was ligated to the digested vector DNA and used for transformation according to the manufacturer's instructions (New England Biolabs, Frankfurt am Main, Germany). Overexpression was carried out in *E. coli* NiCo21 cells in terrific broth (TB) medium supplemented with 100 μg $mL^{-1}$ ampicillin. The cultures were grown at 37 °C and 110 rpm until an optical density $OD_{600}$ = 2. After induction with 1 mM isopropyl-β-D-thiogalactopyranoside (IPTG) the cultures were grown at 16 °C for 18 h and harvested by centrifugation. The bacterial pellets were frozen at −80 °C until further use.

The pellets were resuspended in equilibration buffer containing 20 mM Hepes pH 7.4, 150 mM NaCl, 1 mM dithiothreitol (DTT) and lysed by pulsed sonication using a Branson Digital Sonifier SFX 250 (Emerson, Dietzenbach, Germany) with four cycles, a total time of 2 min, 0.5 s on/off, and 40% amplitude. Centrifugation and filtration were used to clear the lysate prior to purification *via* immobilized metal ion chromatography (IMAC) using an ÄKTApure platform (Cytiva, Freiburg, Germany). The lysate was loaded at 2 mL $min^{-1}$ onto four connected HisTrap excel 5 mL columns equilibrated with equilibration buffer. The loaded columns were washed extensively with equilibration buffer, and 5% elution buffer at 5 mL $min^{-1}$ (20 mM Hepes pH 7.4, 150 mM NaCl, 250 mM imidazole, 1 mM DTT) in order to remove impurities. The fluorescently tagged protein was eluted with 100% elution buffer at 2 mL $min^{-1}$ and fractions were collected.

To cleave both the fluorescent- and the $His_6$-tag, the protein was incubated with TEV protease in a ratio 1 : 100 (w/w protease : protein) and dialyzed against equilibration buffer at 4 °C for 16 h. The solution was loaded onto one HisTrap excel 5 mL column equilibrated with equilibration buffer at 2 mL $min^{-1}$. The flow-through, containing $BCL11B_{42–94}$ species, was collected, and the tags were eluted with 100% elution buffer. Ensuring the purity of $BCL11B_{42–94}$ WT and respective mutants, the proteins were analyzed with reducing 16% tricine SDS-PAGE and analytical size exclusion chromatography.

For experiments with metal ion free protein, $BCL11B_{42–94}$ was dialyzed at 4 °C overnight against 10 mM glycine pH 2.5, 150 μM tris(2-carboxyethyl)phosphine (TCEP) before dialyzing overnight against the respective measurement buffer at 4 °C. For $BCL11B_{42–94}$ H76C, the protein was incubated with a 10-times excess of *N*,*N*,*N*′,*N*′-tetrakis(2-pyridinylmethyl)-1,2-ethanediamine (TPEN) for 48 h at 37 °C, then dialyzed overnight against the respective measurement buffer at 4 °C.

### Size exclusion chromatography

Analytical size exclusion chromatography (SEC) was carried out on an ÄKTAmicro platform (GE Healthcare, Freiburg, Germany)

equipped with a Superdex 200 Increase 3.2/300 column. Apparent sizes were determined through a calibration standard curve (Fig. S1) using protein standards provided by the manufacturer.

### Circular dichroism spectroscopy

Circular dichroism (CD) spectroscopy spectra of 250 μg $mL^{-1}$ protein in 10 mM Tris pH 7.4, 150 mM NaF, 150 μM TCEP were each recorded at 25 °C in a 1 mm path-length quartz glass cuvette (Hellma, Müllheim, Germany) using a Chirascan V100 Circular Dichroism Spectrometer (Applied Photophysics Ltd, Leatherhead, UK). Three repeats were measured from 190 to 250 nm and a bandwidth of 1 nm and averaged. The pH value of the buffer was adjusted using sulfuric acid to ensure chloride free conditions. The respective metal ions ($Co^{2+}$ and $Zn^{2+}$) were each added as $CoSO_4$, and $ZnSO_4$ ensuring a 2-fold excess to saturate the zinc finger domains. Deconvolution of the spectra was carried out using the online platform **https://bestsel.elte.hu/**.[37]

### Isothermal titration calorimetry

Isothermal titration calorimetry (ITC) experiments were carried out using a MicroCal PEAQ-ITC (Malvern Panalytical, Kassel, Germany). 20 μM of $BCL11B_{42–94}$ species were placed in the sample cell and 200 μM of the respective metal ion solution ($CoSO_4$, $ZnSO_4$) in the syringe. Titrations were carried out at 25 °C with 30 injections of 1 μL for 2 s, 60 s initial delay, 150 s spacing and a stirring speed of 750 rpm. The feedback mode was set to high, and the reference power to 3 μcal $s^{-1}$. Evaluation of the data was carried out using the MicroCal PEAQ-ITC Analysis Software Version 1.21 (Malvern Panalytical).

### UV-vis spectroscopy

Metal ion titrations of the $BCL11B_{42–94}$ WT and mutants were carried out using an UV-vis spectrometer Specord 50Plus (Analytik Jena, Jena, Germany) at 25 °C. To 4–8 μM of $BCL11B_{42–94}$ species (in 20 mM MES pH 6.5, 150 mM NaCl, 150 μM TCEP), $CoSO_4$ or $ZnSO_4$ were each added in 0.4–0.8 μM steps until at least two-times excess. UV-vis spectra were recorded from 500 to 800 nm in 0.1 nm steps and a scanning speed of 1 nm $s^{-1}$. For data evaluation, the spectra were blank-, volume-, and baseline corrected. The spectra were smoothed using a Savitzky–Golay filter and a window size of 50. To determine the affinity of the $BCL11B_{42–94}$ to $Co^{2+}$, the fraction bound portion $f_b$ was calculated for the absorption at 652 nm (eqn (1)):

$$f_b = \frac{A_x - A_{min}}{A_{max} - A_{min}} \quad (1)$$

where $A_x$ is the absorption at a specific $Co^{2+}$ concentration, $A_{min}$ is the minimum absorption, and $A_{max}$ is the maximum absorption. The displayed fraction bound $f_b$ data were fitted to Morrison's quadratic equation (eqn (2)):[38]

$$f_b = \frac{(P + I + K_D) - \sqrt{(P + I + K_D)^2 - 4PI}}{2P} \quad (2)$$

where $P$ is the protein concentration, $I$ is the metal ion concentration, and $K_D$ is the dissociation constant. For the determination of the dissociation rate of the $BCL11B_{42–94}(Co^{2+})$ complex, a 10-fold excess of $Zn^{2+}$ was added to the cobalt saturated zinc finger domain and the absorption at 652 nm was observed over time. Eqn (3) was used to fit the experimental data and determine $k_{off}$, with absorption $A_t$ at time $t$, initial absorption $A_0$, $c$ as baseline absorption after dissociation is completed, and $k_{off}$ as dissociation rate constant with eqn (3):

$$A_t = A_0 e^{-k_{off} t} + c \quad (3)$$

Dissociation rate constants were displayed as half-lives determined with eqn (4):

$$t_{1/2} = \frac{\ln(2)}{k_{off}} \quad (4)$$

## Results and discussion

Following up on our previous findings that wild-type (WT) $BCL11B_{42–94}$ forms tetramers and some mutants show the formation of only dimers,[32] we aimed to characterize the WT zinc finger domain and some selected mutants regarding their structural dependence on zinc and their zinc binding properties. In our published molecular dynamics simulations data that revealed the tetrameric zinc finger complex (Fig. 1A), we used a shortened sequence (Fig. 1B, purple), removing the very flexible N- and C-termini. The experiments presented here were carried out using a longer sequence, yielding the $BCL11B_{42–94}$ zinc finger domain (Fig. 1B, black). We focused on the WT domain and three selected mutants (Fig. 1, colored). $BCL11B_{42–94}$ WT is a CCHC type zinc finger domain, as well as I70A (Fig. 1, red), which is located in the hydrophobic interface of two β-dimers,[32] whereas C81H (Fig. 1, blue) renders a C2H2 zinc finger, and H76C (Fig. 1, yellow) a CCCC zinc finger motif.

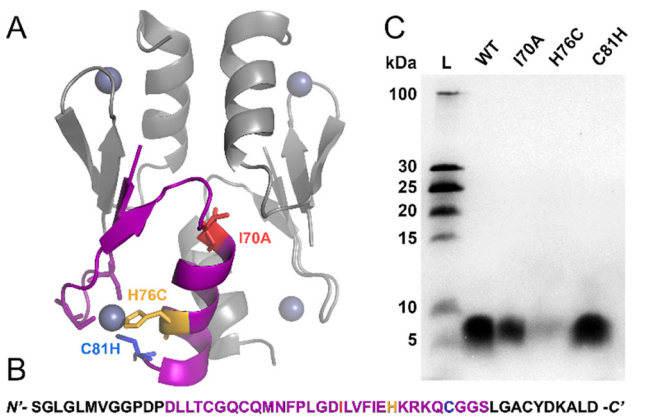


Fig. 1 Structure and sequence of $BCL11B_{42–94}$ wild-type and mutants. (A) Model structure of tetrameric $BCL11B_{42–94}$.[38] A monomer of the N-terminal BCL11B zinc finger domain is depicted in purple, with mutations highlighted in red (I70A), yellow (H76C), and blue (C81H). Zinc ions are colored in metallic blue, and the other monomers of the tetramer are depicted in gray. (B) Sequence of the used $BCL11B_{42–94}$ domain in experiments (black), and in MD simulations[38] (purple). Mutations are colored accordingly. (C) Reducing tricine SDS-PAGE of the WT and mutants. Lane L corresponds to Ladder.

Reducing tricine SDS-PAGE verified purity and the existence of monomers under reducing conditions (Fig. 1C). The fainter band observed for H76C can be attributed to the reduced concentration of the mutant. The purification yield of H76C was low compared to the other three species (data not shown).

### $Zn^{2+}$ dictates the multimerization state and proper folding of $BCL11B_{42–94}$

To gain insights into the size of the zinc finger complex of $BCL11B_{42–94}$ WT and mutants in the presence and in the absence of $Zn^{2+}$, we used analytical size exclusion chromatography (Fig. 2A–D and Fig. S1). The chromatograms revealed that all the examined species showed the formation of larger complexes in the presence of zinc (solid lines) and decreased complex sizes in its absence (dashed lines). With the addition of $Zn^{2+}$, or $Co^{2+}$ (data not shown), the previous complex size could be restored (dotted lines).

As published previously,[32] we found here that the WT (Fig. 2A) and C81H (Fig. 2B) form larger complexes than I70A (Fig. 2C). It appears that H76C (Fig. 2D) is of similar size to I70A. Using a calibration curve (Fig. S1), the calculated complex sizes for all four examined species very roughly exhibit a 2 : 1 ratio each when measured with $Zn^{2+}$ (following expression, with added $Zn^{2+}$) and in the absence of ions.

The precise molecular weight determination using this column proved challenging. The proteins consistently eluted at the column's lower size exclusion limit. The column's reduced bed volume resulted in a significant correlation between even minute variations in elution volume and substantial changes in the calculated molecular weight. Despite this limitation, it is noteworthy that zinc-free WT and C81H complexes appeared to be the same size as zinc-bound I70A and H76C complexes, indicating dimer formation even in the absence of zinc for these variants (Fig. S1).

In order to examine the secondary structure of $BCL11B_{42–94}$ WT, I70A, H76C, and C81H circular dichroism spectra were recorded in the presence and in the absence of $Zn^{2+}$ (Fig. S2). We already showed that $BCL11B_{42–94}$ WT exhibits the typical ββα-fold for zinc finger domains in the presence of zinc.[32,36] C81H shows the same spectrum with typical α-helical peaks at 208 and 228 nm. CD spectra of the mutants I70A and H76C already show (partly) unfolded zinc finger domains even in the presence of zinc, indicated by the peak shift to around 205 nm and less prominent peaks characteristic of helical folds in general.[39,40] With the removal of the central zinc ions, a structural change is being observed, indicating the unfolding of the domains. The peaks observed at 228 nm are no longer visible, and the peaks at 208/205 nm shift to 200 nm. With the addition of $Zn^{2+}$, the native zinc finger fold could be restored in all $BCL11B_{42–94}$ species. Both the influence on the complex size and the secondary structure of the $BCL11B_{42–94}$ domains of the absence/presence of $Zn^{2+}$ are reversible, highlighting the structural dynamics of the small N-terminal zinc finger domain.

For the WT, I70A, and C81H, the qualitative changes in the CD spectra when $Zn^{2+}$ is removed are very prominent. H76C displays only very slight changes in the secondary structure. Therefore, secondary structure changes were quantified by deconvolution (Fig. 3A and Table S1).

The deconvolution data confirm the qualitatively visible secondary structure changes of the spectra and are similar to those observed in other zinc finger domains.[41–44] With $Zn^{2+}$, all four species exhibit a helical content of around 10%, whereas these values drop to 1–5% when zinc ions are removed. This was also observed in other zinc finger domains.[39,44] Additionally, the parallel sheet content decreases to zero when $Zn^{2+}$ is

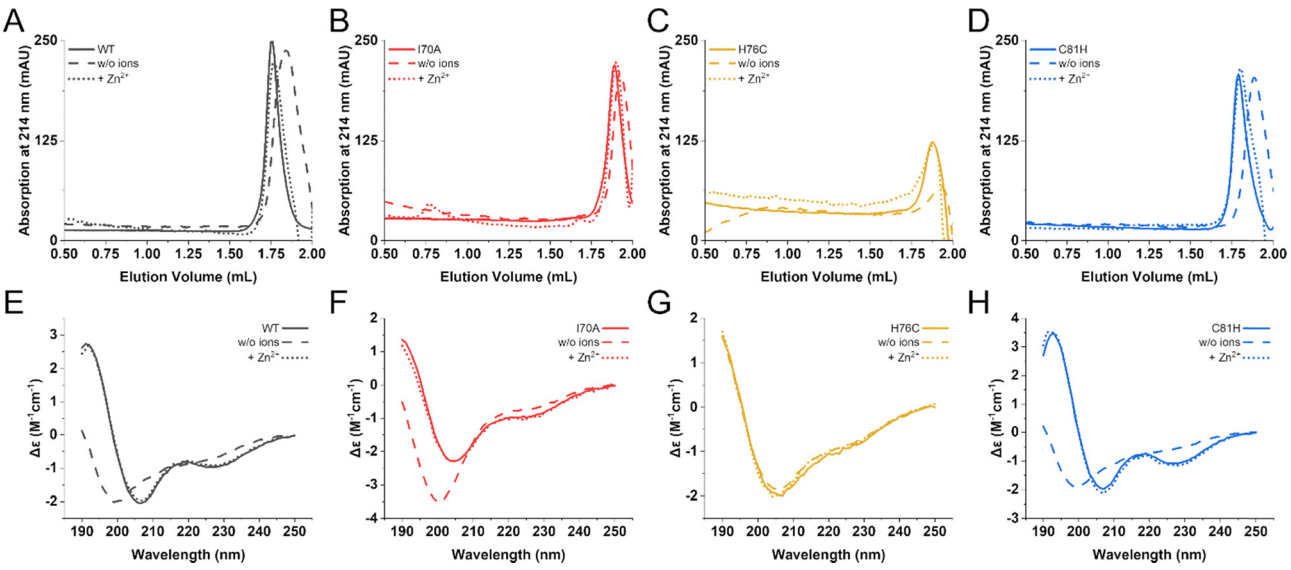


Fig. 2 Zinc dependence of the complex size and secondary structure folding of $BCL11B_{42–94}$ WT and mutants. (A)–(D) Analytical size exclusion chromatography data and (E)–(H) circular dichroism spectra of WT (A) and (E), I70A (B) and (F), H76C (C) and (G), and C81H (D) and (H). Solid lines represent the proteins after expression with coordinated $Zn^{2+}$. Dashed lines correspond to data after zinc was removed, and dotted lines after $Zn^{2+}$ was added again.

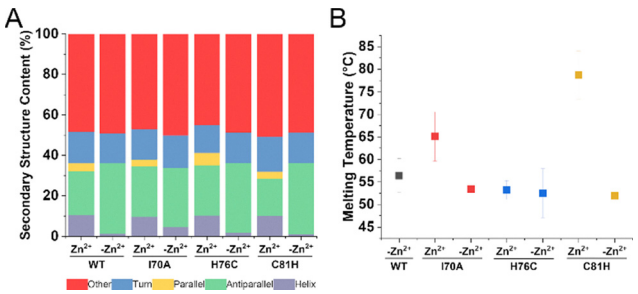


Fig. 3 (A) Secondary structure content of BCL11B$_{42-94}$ WT, I70A, H76C, and C81H each in the presence (+$Zn^{2+}$) and in the absence (−$Zn^{2+}$) of zinc ions. Deconvolution was carried out using *BeStsel.com*.[36] (B) Melting temperatures for BCL11B$_{42-94}$ WT, I70A, H76C, and C81H each with (+$Zn^{2+}$) and without (−$Zn^{2+}$) zinc ions determined using circular dichroism spectroscopy. Precise values for the secondary structure content and melting temperatures with standard deviations are displayed in Table S1.

removed, contributing to the observation of the domain's unfolding. Overall, we see very similar quantitative data after deconvolution. With CD spectroscopy we were not able to distinguish between tetramers or dimers, neither in the qualitative, nor in the quantitative data.

The central zinc ion stabilizes the small zinc finger domain in its structure and also the multimeric complex formation. When $Zn^{2+}$ is removed, the well-defined structure cannot be maintained. The structure is destabilized and the zinc finger fold collapses into a less ordered form, and therefore also the multimeric complex, leading to a decrease in complex size. This observation has been made for other zinc fingers.[45]

In the case of WT and C81H, it seems like the complex is not decreased to its monomer (Fig. S1, ref. 32). There might be several explanations for that. The structure of this small domain still might be well-ordered enough to enable the formation of dimer species. However, we also cannot confirm that the central zinc ions were removed completely, or exclude that the free cysteines form disulfide bridges, even in the presence of a reducing agent. For I70A and H76C, the dissociation from dimers to monomers appears to be the case. The determination of melting points (Fig. 3B and Fig. S3 and Table S1) using CD spectroscopy revealed stable domains for all constructs, both in the presence and in the absence of zinc.

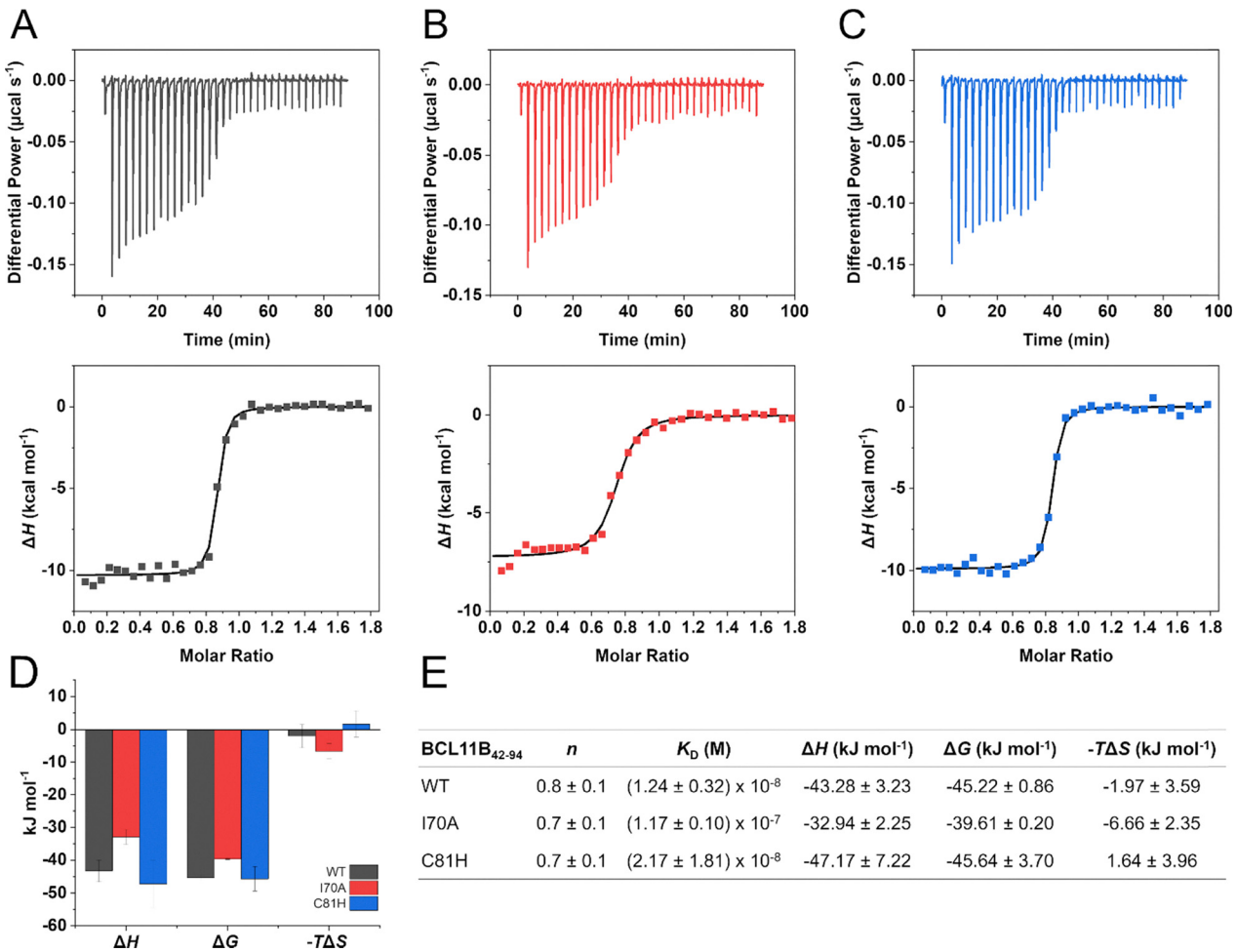


| BCL11B$_{42-94}$ | *n* | $K_D$ (M) | Δ*H* (kJ mol$^{-1}$) | Δ*G* (kJ mol$^{-1}$) | -*T*Δ*S* (kJ mol$^{-1}$) |
|---|---|---|---|---|---|
| WT | 0.8 ± 0.1 | (1.24 ± 0.32) x $10^{-8}$ | -43.28 ± 3.23 | -45.22 ± 0.86 | -1.97 ± 3.59 |
| I70A | 0.7 ± 0.1 | (1.17 ± 0.10) x $10^{-7}$ | -32.94 ± 2.25 | -39.61 ± 0.20 | -6.66 ± 2.35 |
| C81H | 0.7 ± 0.1 | (2.17 ± 1.81) x $10^{-8}$ | -47.17 ± 7.22 | -45.64 ± 3.70 | 1.64 ± 3.96 |

Fig. 4 Isothermal titration calorimetry data of BCL11B$_{42-94}$ (A) WT, (B) I70A, (C) C81H and their interaction with $Zn^{2+}$. Experimental data were fitted with a 1 : 1 binding site model. (D) Thermodynamic parameters of BCL11B$_{42-94}$ variants. (E) Summary of kinetic and thermodynamic parameters determined using ITC. All values represent mean ± standard deviations of at least three independent experiments.

For the WT, no melting point in the presence of $Zn^{2+}$ could be determined in the measured range, whereas we determined melting temperatures of 65.1 °C, 53.2 °C, and 78.7 °C for I70A, H76C, and C81H, respectively. Without the stabilizing central ion, all variants of $BCL11B_{42-94}$ are less stable than their $Zn^{2+}$-stabilized counterparts, exhibiting melting temperatures around 50–55 °C. We assume that $Zn^{2+}$ stabilizes the monomeric domain itself, and the larger complex formation (tetramer/dimer). In the absence of the stabilizing ion and the complex dissociated to dimer/monomer size, the stability also decreases. WT and C81H have higher melting temperatures compared to I70A and H76C, showing that the tetramer complex is more stable than the dimer complex. H76C is slightly more stable with $Zn^{2+}$ than without, and possesses the lowest melting temperature among the examined species, thereby being the least stable. This observation is in line with the observations we made during the expression and purification of this mutant.

### Dimeric complexes have lower affinity to metal ions than tetrameric complexes

Isothermal titration calorimetry experiments with $BCL11B_{42-94}$ WT, I70A, and C81H were carried out in order to determine affinities of the interaction with their central zinc ions (Fig. 4A–C), as well as for the thermodynamic characterization of the coordination (Fig. 4D). Unfortunately, the mutant H76C did not result in any binding with either $Zn^{2+}$ or $Co^{2+}$, therefore, the thermodynamic data could not be evaluated. We suspect the free cysteines are oxidized throughout the experiments or form disulfide bonds, and therefore are not available for metal ion coordination. The WT and C81H exhibit similar affinities to $Zn^{2+}$, with the WT binding slightly stronger. In contrast, the dimeric mutant I70A shows lower affinity, even though I70A has the same CCHC binding motif as the WT. This finding suggests a cooperative effect between tetramerization and zinc binding, and the differences may also arise from varieties in the so-called second coordination sphere.[46]

The thermodynamic parameters (Fig. 4D and E) reveal similar reaction enthalpy ($\Delta H$) and free enthalpy ($\Delta G$) values. The coordination of $Zn^{2+}$ to the $BCL11B_{42-94}$ is enthalpically driven, emphasized by the clearly negative enthalpies. The strongly negative values for the free enthalpy are also typical for zinc finger domains, as well as slightly negative or positive entropy values.[47,48] With the apparent binding affinity $K_{Dapp}$ being smaller than the used protein concentration, we can only conclude that $K_D < 100$ nM for each domain, which is in line with the observed affinities of other zinc fingers to $Zn^{2+}$.[46] Sénèque *et al.*[46] also claim that affinities cannot be determined by direct titration, and that these are always underestimated with this approach. The same applies to the determined thermodynamic parameters. Additionally, the apparent binding enthalpy here is most likely composed of enthalpy for zinc binding, the enthalpy for multimer formation, and changes in enthalpy of buffer protonation.[49]

Notably, the determined stoichiometry $n$ is not equivalent to 1 for all domains, which would have been expected differently. It is most likely that during the process of zinc removal dialysis, the $Zn^{2+}$ ions were not completely removed. Alternatively, following their removal, the cysteine residues, which have been shielded by the bound zinc ions, underwent partial oxidation.[50,51]

### $BCL11B_{42-94}$ adopts a tetrahedral geometry when coordinating $Co^{2+}$

We aimed to compare the affinities of zinc fingers for $Co^{2+}$ from ITC with UV-vis measurements, and to gain insights into dissociation rates of the $BCL11B_{42-94}$–$Co^{2+}$ complexes. Therefore, UV-vis spectra of the $BCL11B_{42-94}$ zinc finger domains titrated with $Co^{2+}$ were recorded (Fig. 5). Analogous to ITC, affinities of H76C to $Co^{2+}$ could not be determined. For the determination of the complex half-lives, the mutants were directly saturated with $Co^{2+}$ after zinc removal. The diamagnetic ion $Zn^{2+}$ possesses a $[Ar]3d^{10}$ electron configuration, and therefore, is spectroscopically silent. In contrast, $Co^{2+}$ occupies the same tetrahedral coordination geometry as $Zn^{2+}$, but allows for the observation of d–d transitions when coordinated by His/Cys. Additionally, $Co^{2+}$ and $Zn^{2+}$ exhibit almost identical ionic radii, with values of 0.58 Å and 0.60 Å, respectively.[52] Because $Zn^{2+}$ is a spectroscopically silent ion in the visible region of the electromagnetic spectrum, $Co^{2+}$ was used as a spectroscopic probe for the zinc site.[39,53] The d–d absorption bands ranging from 500 to 800 nm are indicative of a tetrahedral coordination geometry for the three zinc fingers with high extinction coefficients.[54,55] Therefore, substituting $Zn^{2+}$ with $Co^{2+}$ in the tested mutations does not affect the structural properties of the $BCL11B_{42-94}$ zinc finger domain.

With increasing $Co^{2+}$ concentrations and in the saturated complex, three peaks in the range from 500–800 nm were observed for WT (Fig. 5A), and I70A (Fig. 5B), whereas two

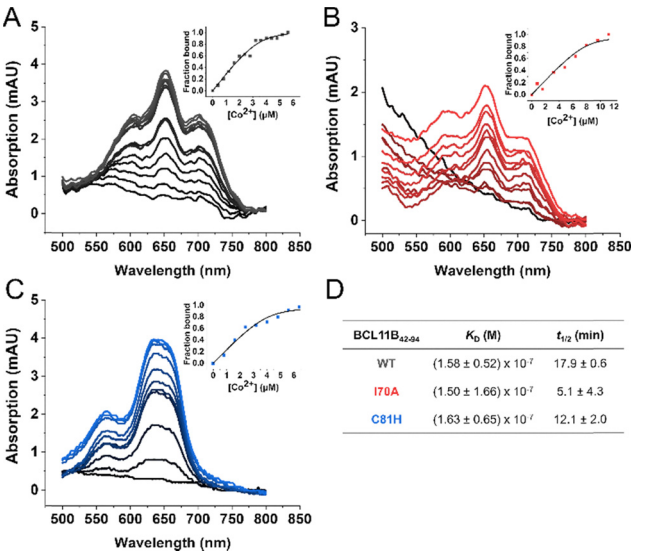


Fig. 5 UV-vis spectroscopy measurements of $BCL11B_{42-94}$ (A) WT, (B) I70A, and (C) C81H. The insets show fraction bound values calculated from absorption at 652 nm against $[Co^{2+}]$. (D) Summary of determined binding affinity constants KD of the $BCL11B_{42-94}$ $Co^{2+}$ complexes, and dissociation rates expressed as half-lives.

peaks are visible for C81H (Fig. 5C). This is in line with the proposition of Sivo *et al.*, who suggested that maxima in the region of 500–700 nm indicate the number of coordinating cysteine ligands.[56] In the order WT, I70A, C81H, a blue-shift in d–d transition bands is visible, with the observed peaks being shifted to higher energies as the coordinating cysteine residues are decreased.[57]

The determined $K_D$ values of WT, I70A, and C81H are very similar, but differ in comparison with these values obtained from ITC (Fig. S4) by a magnitude of 10, except for C81H. Here, the affinity to $Co^{2+}$ appears to be higher for WT and I70A in comparison to the ITC experiments. The determined dissociation rate constants $k_{off}$ are displayed as complex half-lives $t_{1/2}$ (Fig. 5D) and show that the WT has the highest half-life, followed by C81H, and I70A. I70A, although endowed with a CCHC zinc finger motif as the WT, exhibits the shortest half-life. This suggests that the WT and C81H have more structural stability through its tetrameric nature and thus, slower dissociation rates for bound ions, and I70A with its dimeric domain less structural stability of the coordinated metal ion.

## Conclusions

In this study, we highlight the influence of $Zn^{2+}$ on the structural integrity and stability of the N-terminal zinc finger domain of BCL11B. The $BCL11B_{42–94}$ WT and its zinc finger motif mutant C81H form tetramers in the presence of $Zn^{2+}$, whereas the mutants I70A and H76C form dimers. For all tested variants, the removal of $Zn^{2+}$ resulted in the destabilization of the secondary structure of proteins and leads to a decrease in complex size, but both can be restored with the re-addition of $Zn^{2+}$. ITC measurements revealed a higher affinity of the tetrameric domains WT, and C81H to $Co^{2+}$ and $Zn^{2+}$ compared to the dimeric I70A. Importantly, the reduced zinc binding affinity observed for the I70A mutant, despite this residue being outside the direct zinc coordination sphere, provides compelling evidence for a cooperative interplay between BCL11B's multimerization state and the stability of its zinc binding. This finding suggests that the higher-order assembly directly contributes to the stability of the zinc finger's zinc coordination and *vice versa*. $BCL11B_{42–94}$ WT exhibits the highest melting temperature and the longest half-life, highlighting its increased stability compared to its mutants. UV-vis spectroscopy further confirmed the tetrahedral binding geometry of the zinc fingers to $Co^{2+}$, indicating that the structural core motif is preserved across mutations. Furthermore, the study demonstrated that d–d transition shifts to higher energy when the number of cysteine residues is reduced.

Collectively, our findings further emphasize the significance of the tetrameric zinc finger domain on its structural integrity and stability and suggest zinc key modulator function of its functional conformation. Overall, our findings establish that the central zinc ion is not only critical for the proper folding of the $BCL11B_{42–94}$ domain but also for its ability to form higher-order complexes, which in turn confers greater structural stability and metal ion affinity. This comprehensive biophysical characterization lays crucial groundwork for potentially novel therapeutic approaches targeting BCL11B. Specifically, the reversible and zinc-dependent multimerization identified in this study offers a promising avenue for modulating BCL11B function. However, for these findings to translate into viable drug discovery strategies, future cellular studies will be essential to demonstrate the functional consequences of BCL11B dissociation to either a dimer or a monomer on its expression levels and overall cellular activity.

At present, we cannot definitively distinguish whether the degradation of $BCL11B_{42–94}$ WT is limited to dimer formation due to residual zinc ions after our removal protocol, or whether an unfolded domain can provide sufficient structure and stability to form functional dimers. Addressing this issue will be a vital further step in harnessing the therapeutic potential of BCL11B multimerization.

## Author contributions

Conceptualization – A. S., C. A. S. and M. D.; data curation – A. S. and F. N.; formal analysis – A. S.; funding acquisition – C. A. S.; investigation – A. S.; methodology – A. S. and F. N.; project administration – C. A. S. and M. D.; resources – M. D. and C. A. S.; supervision – C. A. S. and M. D.; validation – A. S., F. N. and P. G.; visualization – A. S., writing – original draft – A. S.; writing – review and editing – F. N., P. G., C. A. S., M. D. All authors have read and agreed to the published version of the manuscript.

## Conflicts of interest

There are no conflicts to declare.

## Data availability

The data supporting this article have been included as part of the supplementary information (SI). Supplementary information is available. See DOI: **https://doi.org/10.1039/d5cp02933c**.

## Acknowledgements

Publication fees were supported by the University Library of the University of Greifswald as part of a transformative agreement with the Royal Society of Chemistry.

## Notes and references

1 R. S. Brown, C. Sander and P. Argos, The primary structure of transcription factor TFIIIA has 12 consecutive repeats, *FEBS Lett.*, 1985, **186**(2), 271–274.
2 T. A. Hartshorne, H. Blumberg and E. T. Young, Sequence homology of the yeast regulatory protein ADR1 with Xenopus transcription factor TFIIIA, *Nature*, 1986, **320**(6059), 283–287.

3 R. Schuh, W. Aicher, U. Gaul, S. Côte, A. Preiss and D. Maier, *et al.*, A conserved family of nuclear proteins containing structural elements of the finger protein encoded by Krüppel, a Drosophila segmentation gene, *Cell*, 1986, **47**(6), 1025–1032. Available from: **https://linkinghub.elsevier.com/retrieve/pii/0092867486908172**.
4 A. Klug, The discovery of zinc fingers and their applications in gene regulation and genome manipulation, *Annu. Rev. Biochem.*, 2010, **79**, 213–231.
5 A. Klug, The discovery of zinc fingers and their applications in gene regulation and genome manipulation, *Annu. Rev. Biochem.*, 2010, **79**(1), 213–231. Available from: **https://www.annualreviews.org/doi/10.1146/annurev-biochem-010909-095056**.
6 Z. Kamaliyan and T. L. Clarke, Zinc finger proteins: guardians of genome stability, *Front. Cell. Dev. Biol.*, 2024, **12**, 1–8. Available from: **https://www.frontiersin.org/articles/10.3389/fcell.2024.1448789/full**.
7 G. Bulaj, T. Kortemme and D. P. Goldenberg, Ionization–Reactivity Relationships for Cysteine Thiols in Polypeptides, *Biochemistry*, 1998, **37**(25), 8965–8972. Available from: **https://pubs.acs.org/doi/10.1021/bi973101r**.
8 J. N. Smith, J. T. Hoffman, Z. Shirin and C. J. Carrano, H-Bonding Interactions and Control of Thiolate Nucleophilicity and Specificity in Model Complexes of Zinc Metalloproteins, *Inorg. Chem.*, 2005, **44**(6), 2012–2017. Available from: **https://pubs.acs.org/doi/10.1021/ic048630f**.
9 Y.-M. Lee and C. Lim, Factors controlling the reactivity of zinc finger cores, *J. Am. Chem. Soc.*, 2011, **133**(22), 8691–8703. Available from: **https://pubs.acs.org/doi/10.1021/ja202165x**.
10 M. Laitaoja, J. Valjakka and J. Jänis, Zinc coordination spheres in protein structures, *Inorg. Chem.*, 2013, **52**(19), 10983–10991.
11 J. H. Laity, B. M. Lee and P. E. Wright, Zinc finger proteins: New insights into structural and functional diversity, *Curr. Opin. Struct. Biol.*, 2001, **11**(1), 39–46.
12 S. S. Krishna, Structural classification of zinc fingers: SURVEY AND SUMMARY, *Nucleic Acids Res.*, 2003, **31**(2), 532–550. Available from: **https://academic.oup.com/nar/article-lookup/doi/10.1093/nar/gkg161**.
13 M. Cassandri, A. Smirnov, F. Novelli, C. Pitolli, M. Agostini and M. Malewicz, *et al.*, Zinc-finger proteins in health and disease, *Cell Death Discovery*, 2017, **3**, 1.
14 J. Jen and Y. C. Wang, Zinc finger proteins in cancer progression, *J. Biomed. Sci.*, 2016, **23**(1), 1–9, DOI: **10.1186/s12929-016-0269-9**. Available from: .
15 J. Zhao, D. Wen, S. Zhang, H. Jiang and X. Di, The role of zinc finger proteins in malignant tumors, *FASEB J.*, 2023, **37**(9), 1–15. Available from: **https://faseb.onlinelibrary.wiley.com/doi/10.1096/fj.202300801R**.
16 C. Abbehausen, Zinc finger domains as therapeutic targets for metal-based compounds – an update, *Metallomics*, 2019, **11**(1), 15–28, DOI: **10.1039/C8MT00262B**. Available from: .
17 Y. Cheng, H. Geng, S. H. Cheng, P. Liang, Y. Bai and J. Li, *et al.*, KRAB Zinc Finger Protein ZNF382 Is a Proapoptotic Tumor Suppressor That Represses Multiple Oncogenes and Is Commonly Silenced in Multiple Carcinomas, *Cancer Res.*, 2010, **70**(16), 6516–6526. Available from: **https://aacrjournals.org/cancerres/article/70/16/6516/559394/KRAB-Zinc-Finger-Protein-ZNF382-Is-a-Proapoptotic**.
18 C. Tao, J. Luo, J. Tang, D. Zhou, S. Feng and Z. Qiu, *et al.*, The tumor suppressor Zinc finger protein 471 suppresses breast cancer growth and metastasis through inhibiting AKT and Wnt/β-catenin signaling, *Clin. Epigenet.*, 2020, **12**(1), 173. Available from: **https://doi.org/10.1186/s13148-020-00959-6**.
19 J. Zhang, J. Luo, H. Jiang, T. Xie, J. Zheng and Y. Tian, *et al.*, The Tumor Suppressor Role of Zinc Finger Protein 671 (ZNF671) in Multiple Tumors Based on Cancer Single-Cell Sequencing, *Front. Oncol.*, 2019, **9**, 1–11. Available from: **https://www.frontiersin.org/article/10.3389/fonc.2019.01214/full**.
20 H. K. Permatasari, S. Nakahata, T. Ichikawa, Y. R. Fauzi, H. Kiyonari and K. Shide, *et al.*, Oncogenic isoform switch of tumor suppressor BCL11B in adult T-cell leukemia/lymphoma, *Exp. Hematol.*, 2022, **111**, 41–49. Available from: **https://doi.org/10.1016/j.exphem.2022.04.004**.
21 Y. Wakabayashi, H. Watanabe, J. Inoue, N. Takeda, J. Sakata and Y. Mishima, *et al.*, Bcl11b is required for differentiation and survival of αβ T lymphocytes, *Nat. Immunol.*, 2003, **4**(6), 533–539.
22 J. P. P. Meijerink, BCL11B, the Cerberus of human leukemia, *Blood*, 2021, **138**(9), 741–743. Available from: **https://ashpublications.org/blood/article/138/9/741/476680/BCL11B-the-Cerberus-of-human-leukemia**.
23 D. M. Su and R. Vankayalapati, A new avenue to cure cancer by turning adaptive immune T cells to innate immune NK cells via reprogramming, *J. Mol. Cell Biol.*, 2010, **2**(5), 237–239.
24 P. Li, S. Burke, J. Wang, X. Chen, M. Ortiz and S. C. Lee, *et al.*, Reprogramming of T cells to natural killer-like cells upon Bcl11b deletion, *Science*, 2010, **329**(5987), 85–89.
25 D. I. Albu, D. Feng, D. Bhattacharya, N. A. Jenkins, N. G. Copeland and P. Liu, *et al.*, BCL11B is required for positive selection and survival of double-positive thymocytes, *J. Exp. Med.*, 2007, **204**(12), 3003–3015. Available from: **https://rupress.org/jem/article/204/12/3003/46612/BCL11B-is-required-for-positive-selection-and**.
26 H. Forkel, P. Grabarczyk, M. Depke, S. Troschke-Meurer, S. Simm and E. Hammer, *et al.*, BCL11B depletion induces the development of highly cytotoxic innate T cells out of IL-15 stimulated peripheral blood αβ CD8+ T cells, *Oncoimmunology*, 2022, **11**(1), e2148850. Available from: **https://doi.org/10.1080/2162402X.2022.2148850**.
27 L. J. Zhang, W. K. Vogel, X. Liu, A. Topark-Ngarm, B. L. Arbogast and C. S. Maier, *et al.*, Coordinated regulation of transcription factor bcl11b activity in thymocytes by the Mitogen-activated Protein Kinase (MAPK) pathways and protein sumoylation, *J. Biol. Chem.*, 2012, **287**(32), 26971–26988, DOI: **10.1074/jbc.m112.344176**. Available from: .
28 A. Oshiro, H. Tagawa, K. Ohshima, K. Karube, N. Uike and Y. Tashiro, *et al.*, Identification of subtype-specific genomic alterations in aggressive adult T-cell leukemia/lymphoma, *Blood*, 2006, **107**(11), 4500–4507.

29 M.-T. Daher, P. Bausero, O. Agbulut, Z. Li and A. Parlakian, Bcl11b/Ctip2 in Skin, Tooth, and Craniofacial System, *Front. Cell. Dev. Biol.*, 2020, **8**, 1–15. Available from: **https://www.frontiersin.org/articles/10.3389/fcell.2020.581674/full**.

30 X. Gu, Y. Wang, G. Zhang, W. Li and P. Tu, Aberrant expression of BCL11B in mycosis fungoides and its potential role in interferon-induced apoptosis, *J. Dermatol.*, 2013, **40**(8), 596–605. Available from: **https://onlinelibrary.wiley.com/doi/10.1111/1346-8138.12160**.

31 P. Grabarczyk, P. Winkler, M. Delin, P. K. Sappa, S. Bekeschus and P. Hildebrandt, *et al.*, The N-Terminal CCHC Zinc Finger Motif Mediates Homodimerization of Transcription Factor BCL11B, *Mol. Cell Biol.*, 2018, **38**(5), 1–17. Available from: **https://journals.asm.org/doi/10.1128/MCB.00368-17**.

32 A. Susemihl, N. Geist, P. Grabarczyk, C. A. Schmidt, M. Delcea and L. Schulig, Double the Double: Revisiting BCL11B's Multimerization, *Proteins: Struct., Funct., Bioinf.*, 2025, 1205–1211.

33 G. Zheng, M. Yin, S. Mehta, I.-T. Chu, S. Wang and A. AlShaye, *et al.*, A tetramer of BCL11A is required for stable protein production and fetal hemoglobin silencing, *Science*, 2024, **386**(6725), 1010–1018. Available from: **https://www.science.org/doi/10.1126/science.adp3025**.

34 J. R. Horton, M. Yu, J. Zhou, M. Tran, R. R. Anakal and Y. Lu, *et al.*, Multimeric transcription factor BCL11A utilizes two zinc-finger tandem arrays to bind clustered short sequence motifs, *Nat. Commun.*, 2025, **16**(1), 3672, DOI: **10.1038/s41467-025-58998-7**. Available from: .

35 B. L. Z. Oh, N. Shimasaki, E. Coustan-Smith, E. Chan, L. Poon and S. H. R. Lee, *et al.*, Fratricide-resistant CD7-CAR T cells in T-ALL, *Nat. Med.*, 2024, **30**(12), 3687–3696, DOI: **10.1038/s41591-024-03228-8**. Available from: .

36 A. Susemihl, F. Nagel, P. Grabarczyk, C. A. Schmidt and M. Delcea, Easy expression and purification of fluorescent N-terminal BCL11B CCHC zinc finger domain, *Molecules*, 2021, **26**(24), 1–11.

37 A. Micsonai, É. Moussong, F. Wien, E. Boros, H. Vadászi and N. Murvai, *et al.*, BeStSel: webserver for secondary structure and fold prediction for protein CD spectroscopy, *Nucleic Acids Res.*, 2022, **50**(W1), W90–W98. Available from: **https://doi.org/10.1093/nar/gkac345**.

38 C. Isernia, E. Bucci, M. Leone, L. Zaccaro, P. Di Lello and G. Digilio, *et al.*, NMR structure of the single QALGGH zinc finger domain from the Arabidopsis thaliana SUPERMAN protein, *ChemBioChem*, 2003, **4**(2–3), 171–180.

39 A. D. Frankel, J. M. Berg and C. O. Pabo, Metal-dependent folding of a single zinc finger from transcription factor IIIA, *Proc. Natl. Acad. Sci. U. S. A.*, 1987, **84**(14), 4841–4845.

40 K. Kluska, J. Adamczyk and A. Krężel, Metal binding properties, stability and reactivity of zinc fingers, *Coord. Chem. Rev.*, 2018, **367**, 18–64. Available from: **https://linkinghub.elsevier.com/retrieve/pii/S0010854517305441**.

41 A. D. Frankel, J. M. Berg and C. O. Pabo, Metal-dependent folding of a single zinc finger from transcription factor IIIA, *Proc. Natl. Acad. Sci. U. S. A.*, 1987, **84**(14), 4841–4845. Available from: **https://pnas.org/doi/full/10.1073/pnas.84.14.4841**.

42 O. F. Ezomo, K. Takahashi, Y. Horie and M. S. Mustak, Circular Dichroism Studies on C-terminal Zinc Finger Domain of Transcription Factor GATA-2, *Yonago Acta Med.*, 2010, 25–28.

43 A. Nomura and Y. Sugiura, Contribution of Individual Zinc Ligands to Metal Binding and Peptide Folding of Zinc Finger Peptides, *Inorg. Chem.*, 2002, **41**(14), 3693–3698. Available from: **https://pubs.acs.org/doi/10.1021/ic025557p**.

44 K. Sakai-Kato, Y. Umezawa, K. Mikoshiba, J. Aruga and N. Utsunomiya-Tate, Stability of folding structure of Zic zinc finger proteins, *Biochem. Biophys. Res. Commun.*, 2009, **384**(3), 362–365, DOI: **10.1016/j.bbrc.2009.04.151**. Available from: .

45 R. Zheng, T. M. Jenkins and R. Craigie, Zinc folds the N-terminal domain of HIV-1 integrase, promotes multimerization, and enhances catalytic activity, *Proc. Natl. Acad. Sci. U. S. A.*, 1996, **93**(24), 13659–13664.

46 O. Sénèque and J.-M. Latour, Coordination Properties of Zinc Finger Peptides Revisited: Ligand Competition Studies Reveal Higher Affinities for Zinc and Cobalt, *J. Am. Chem. Soc.*, 2010, **132**(50), 17760–17774. Available from: **https://pubs.acs.org/doi/10.1021/ja104992h**.

47 S. Ghimire-Rijal and E. L. Maynard, Comparative Thermodynamic Analysis of Zinc Binding to the His/Cys Motif in Virion Infectivity Factor, *Inorg. Chem.*, 2014, **53**(9), 4295–4302. Available from: **https://pubs.acs.org/doi/10.1021/ic402907g**.

48 A. M. Rich, E. Bombarda, A. D. Schenk, P. E. Lee, E. H. Cox and A. M. Spuches, *et al.*, Thermodynamics of Zn 2+ Binding to Cys 2 His 2 and Cys 2 HisCys Zinc Fingers and a Cys 4 Transcription Factor Site, *J. Am. Chem. Soc.*, 2012, **134**(25), 10405–10418. Available from: **https://pubs.acs.org/doi/10.1021/ja211417g**.

49 K. Kluska, A. Chorążewska, M. D. Peris-Díaz, J. Adamczyk and A. Krężel, Non-Conserved Amino Acid Residues Modulate the Thermodynamics of Zn(II) Binding to Classical ββα Zinc Finger Domains, *Int. J. Mol. Sci.*, 2022, **23**, 23.

50 D. levy dan Bree, Purifying Properly Folded Cysteine-rich, Zinc Finger Containing Recombinant Proteins for Structural Drug Targeting Studies: the CH1 Domain of p300 as a Case Example, *Physiol. Behav.*, 2019, **176**(3), 139–148.

51 V. Lebrun, A. Tron, L. Scarpantonio, C. Lebrun, J. Ravanat and J. Latour, *et al.*, Efficient Oxidation and Destabilization of Zn(Cys) 4 Zinc Fingers by Singlet Oxygen, *Angew. Chem., Int. Ed.*, 2014, **53**(35), 9365–9368. Available from: **https://onlinelibrary.wiley.com/doi/10.1002/anie.201405333**.

52 R. D. Shannon, Revised effective ionic radii and systematic studies of interatomic distances in halides and chalcogenides, *Acta Crystallogr., Sect. A*, 1976, **32**(5), 751–767. Available from: **https://journals.iucr.org/paper?S0567739476001551**.

53 O. Sénèque and J. M. Latour, Coordination properties of zinc finger peptides revisited: Ligand competition studies reveal higher affinities for zinc and cobalt, *J. Am. Chem. Soc.*, 2010, **132**(50), 17760–17774.

54 M. Vasak, J. H. R. Kaegi, B. Holmquist and B. L. Vallee, Spectral studies of cobalt(II)- and nickel(II)-metallothionein,

*Biochemistry*, 1981, **20**(23), 6659–6664. Available from: **https://pubs.acs.org/doi/abs/10.1021/bi00526a021**.

55 S. W. May and J. Kuo, Preparation and properties of cobalt(II) rubredoxin, *Biochemistry*, 1978, **17**(16), 3333–3338. Available from: **https://pubs.acs.org/doi/abs/10.1021/bi00609a025**.

56 V. Sivo, G. D'Abrosca, L. Russo, R. Iacovino, P. V. Pedone and R. Fattorusso, *et al.*, Co(II) Coordination in Prokaryotic Zinc Finger Domains as Revealed by UV-Vis Spectroscopy, *Bioinorg. Chem. Appl.*, 2017, **2017**, 1–7. Available from: **https://www.hindawi.com/journals/bca/2017/1527247/**.

57 B. A. Krizek, D. L. Merkle and J. M. Berg, Ligand variation and metal ion binding specificity in zinc finger peptides, *Inorg. Chem.*, 1993, **32**(6), 937–940. Available from: **https://pubs.acs.org/doi/abs/10.1021/ic00058a030**.